This is a preprint, the final version is subject to change, of the American Mineralogist (MSA)
Cite as Authors (Year) Title. American Mineralogist, in press.
(DOI will not work until issue is live.) DOI: http://dx.doi.org/10.2138/am-2017-5616

REVISION 1

Mineralogical controls on antimony and arsenic mobility during tetrahedrite-tennantite weathering at historic mine sites Špania Dolina-Piesky and Ľubietová-Svätodušná, Slovakia

Anežka Borčinová Radková[1 *], Heather Jamieson[1], Bronislava Lalinská-Voleková[2], Juraj Majzlan[3], Martin Števko[4], Martin Chovan[5]

[1]*Department of Geological Sciences and Geological Engineering, Queen's University, Miller Hall, 36 Union Street, Kingston, K7L 3N6, Ontario, Canada*

[2]*Slovak National Museum, Natural History Museum, Vajanského nábr. 2, P.O.BOX 13, 810 06 Bratislava, Slovakia*

[3]*Institute of Geosciences, Burgweg 11, Friedrich-Schiller University, D–07749 Jena, Germany*

[4]*Department of Mineralogy and Petrology, Faculty of Natural Sciences, Comenius University, 6 Mlynska dolina G, SK-842 15 Bratislava, Slovakia*

[5] *Institute of Geological Engineering, Technical University of Ostrava, 17. listopadu, 70833 Ostrava-Poruba, Czech Republic*

*corresponding author: Anezka.radkova@queensu.ca

Abstract

The legacy of copper (Cu) mining at Špania Dolina-Piesky and Ľubietová-Svätodušná (central Slovakia) is waste rock and soil, surface waters, and groundwaters contaminated with antimony (Sb), arsenic (As), Cu and other metals. Copper ore is hosted in chalcopyrite ($CuFeS_2$) and sulfosalt solid solution tetrahedrite-tennantite ($Cu_6[Cu_4(Fe,Zn)_2]Sb_4S_{13}$ - $Cu_6[Cu_4(Fe,Zn)_2]As_4S_{13}$) that show widespread oxidation characteristic by olive-green color secondary minerals. Tetrahedrite-tennantite can be a significant source of As and Sb contamination. Synchrotron-based μ-XRD, μ-XRF, and μ-XANES combined with electron microprobe analyses have been used to determine the mineralogy, chemical composition, element distribution and Sb speciation in tetrahedrite-tennantite oxidation products in waste rock. Our results show that the mobility of Sb is limited by the formation of oxidation products such as tripuhyite and roméite group mineral containing 36.54 wt% Sb for samples where the primary mineral chemical composition is close to tetrahedrite end member. Antimony K edge μ-XANES spectra of these oxidation products indicate that the predominant Sb oxidation state is 5^+. Arsenic and Cu are also hosted by amorphous phases containing 6.23 wt% Sb on average and these are intergrown with tripuhyite and roméite. Antimony in this environment is not very mobile, meaning it is not easily released from solid phases to water, especially compared to As, Cu and S. For samples where the primary sulfosalt is close to tennantite composition, the oxidation products associated with tennantite relicts contain 2.43 wt% Sb and are amorphous. The variable solubility of the secondary minerals that have been identified are expected to influence mobility of Sb and As in near surface-environment.

KEY WORDS

41 tetrahedrite-tennantite weathering, waste rock, antimony, arsenic, supergene minerals, tripuhyite,
42 roméite

43 Introduction

44 Tetrahedrite (ttd) is a complex sulfosalt with a general chemical formula $Cu_6[Cu_4(Fe,Zn)_2]Sb_4S_{13}$
45 and may contain many different elements such as Cu, Ag, Zn, Fe, Cd, Hg, Sb, As, Bi, S, Se and
46 Te (Johnson et al., 1986; Baláž, 2000; Moëlo et al., 2008). There is a complete solid solution
47 between tetrahedrite $Cu_6[Cu_4(Fe,Zn)_2]Sb_4S_{13}$ and tennantite (tnn) $Cu_6[Cu_4(Fe,Zn)_2]As_4S_{13}$ (King,
48 2001; Filippou et al., 2007; Moëlo et al., 2008). In this paper, we will refer to the members of the
49 tetrahedrite-tennantite solid solution (hereafter ttd-tnn) with Sb/(Sb+As) > 0.5 as tetrahedrite and
50 those with this ratio < 0.5 as tennantite. The solid solution of ttd-tnn is commonly found in low-
51 to moderate-temperature hydrothermal veins (e.g. Lynch, 1989; Arlt and Diamond 1998;
52 Vassileva et al., 2014). The high Cu content (40 to 46 wt%) and frequent presence
53 of Ag means that tetrahedrite and tennantite are economically attractive, but the
54 presence of potentially toxic Sb (29 wt% in end-member tetrahedrite) and As (20
55 wt% in end-member tennantite) indicates that the waste from these deposits may be
56 environmentally problematic. Exposure of tetrahedrite and tennantite to oxidizing conditions
57 can result in the mobilization of Sb, As, Cu, S and other elements present in their structure
58 (Wilson et al., 2004; Filippou et al., 2007; Lengke, 2009; Hiller et al., 2013). Environmental
59 mobility is influenced by the formation and stability of secondary phases, depending on the
60 prevalent geochemical conditions.

61 Coprecipitation and absorption of Sb, among many other elements, onto Fe oxides is an
62 important control on the mobility of antimony. If the Sb concentration is sufficiently high,
63 however, Sb secondary minerals will form (Filella et al., 2009). Although Sb secondary minerals

64 are relatively diverse, only a few phases are environmentally important and relatively common
65 (Majzlan et al. 2011; Roper et al., 2012, 2015). If the concentrations of dissolved Sb(V) are
66 elevated, Sb can be immobilized by formation of Sb(V) phases such tripuhyite, which has been
67 identified as an important Sb sink at several tailing impoundments and in oxidation zones of
68 hydrothermal deposits (Diemar et al., 2009; Majzlan et al., 2011; Lalinská-Voleková et al., 2012;
69 Leverett et al., 2012; Bolanz et al., 2013). The ideal chemical formula is $Fe^{3+}Sb^{5+}O_4$, and the
70 crystal structure is tetragonal, with the unit cell dimensions of: a = 4.63 Å, c =3.06Å, V = 65.43
71 $Å^3$, Z = 2 (Berlepsch et al., 2003). The most likely molar ratio in solution for the crystallization
72 of tripuhyite is Fe:Sb 1:2 and wide range of pH values (1-10) are favourable for its formation
73 (Diemar, 2008; Rusinová et al., 2014). Current studies indicate that tripuhyite is able to adsorb or
74 incorporate As (up to 1.88 wt%) while diminishing the Fe content in this mineral, which might
75 cause changes in lattice parameters and unit cell volume (3V = 65.43 – 66.35 $Å^3$) (Rusinová et
76 al., 2014). Tripuhyite is increasingly recognized as a highly insoluble Sb host (Leverett et al.,
77 2012), and has been commonly observed as an alteration product of stibnite, berthierite, or
78 gudmundite in the presence of pyrite and arsenopyrite (e.g. Lalinská-Voleková et al., 2012).
79 Information about tripuhyite as a tetrahedrite oxidation product is rare (Nickel, 1984; Harris et
80 al., 2003; Diemar et al., 2009).

81 In oxidized settings, the mobility of Sb can also be controlled by the precipitation of
82 minerals with the cubic, pyrochlore-like structure (Diemar, 2008; Diemar et al., 2009). These
83 structures are capable of accommodating a wide variety of cations with a general formula A_{2-}
84 $_mB_2X_{6-w}Y_{1-n}$. A is usually a large eight-fold coordinated cation, most commonly Na, Ca, Sr, Pb^{2+},
85 Sn, Sb^{3+}, alternatively a vacancy or a H_2O molecule. B is typically a 6-fold coordinated cation,
86 usually Nb^{5+}, Ti^{4+}, Sb^{5+}, Fe^{3+}, Mg, Si, Al. X is O, OH or F. Y is usually an anion, vacancy or H_2O

(Atencio et al., 2010). Minerals from the roméite group ($Ca_2Sb_2O_7$) belonging to pyrochlore supergroup have been identified in slag residues (Courtin-Nomade, 2012) and tailings (Klimko et al., 2011) resulting from Sb mining activities. To date, comprehensive information about the solubility of the roméite-group minerals is missing.

At most sites where Sb associates with ore minerals, it is accompanied by As. Relative to Sb, under near-neutral and oxidizing conditions, As has a higher affinity for adsorption on Fe oxides such as goethite and ferrihydrite (Bowell, 1994; Lalinská-Voleková et al., 2012; Ritchie et al., 2013). In some cases, under neutral weathering conditions, Ca-Fe arsenates such as yukonite are formed (Walker et al., 2009). Scorodite ($FeAsO_4 \cdot 2H_2O$) is an important product of arsenopyrite weathering, controlling As solubility at pH less than 3 (Flemming et al., 2005; Moldovan and Hendry, 2005, DeSisto et al. 2011). Under circumneutral pH conditions, scorodite is metastable and breaks down to iron hydroxides and adsorbed/aqueous arsenate (Nordstrom et al. 2014).

In this study, our attention is focused on how Sb and As are hosted in the oxidation products of the tetrahedrite-tennantite solid solution in mine-waste piles. Using two historic mining sites with abundant tetrahedrite and tennantite, we characterized the weathering products by electron microprobe analyses and a suite of synchrotron-based microtechniques, such as micro-X-ray diffraction, micro-X-ray fluorescence and micro-X-ray absorption spectroscopy.

Site description

Samples from two abandoned mining areas were studied, the Špania Dolina - Piesky and Ľubietová - Svätodušná, both located in central Slovakia, in the central part of the Western Carpathians.

The **Špania Dolina - Piesky** deposit is situated 1.2 km north of the village of Špania Dolina in Starohorské Mountains (Figure 1). The Cu ores are dispersed in a hydrothermal stockwork of quartz-siderite-sulfide veinlets and impregnations hosted mainly by Permian sandstones and conglomerates (Čillík et al., 1986; Vozárová et al., 2014). Tetrahedrite is the dominant ore mineral (Sejkora et al., 2013) with minor amounts of chalcopyrite and accessory arsenopyrite, bornite, galena, cobaltite, pyrite and sphalerite. Gangue minerals include quartz, Fe-dolomite, siderite, barite and calcite (Novotný, 1960; Regásek, 1973; Michňová and Ozdín, 2010). The deposit has a well-developed oxidation zone with a variety of secondary minerals reported in Table 1, making this area popular among mineral collectors. The beginning of the mining activities dates back to the end of Neolithic era (Žebrák et al., 1986). The most intensive mining period was during 15th and 16th century when this deposit was an important Cu and Ag producer for central Europe. Mining and exploration activities continued until 1985 and since then the waste dumps have remained mostly undisturbed (Čillík et al., 1986; Kusein and Maťová, 2002) with the exception of reclamation work at a few of the waste rock piles. Unsorted waste rock material is accumulated in dumps at several sites in valleys and around the former shafts. Numerous waste rock piles cover area more than 1 km in length and 150 m wide (Sejkora et al., 2013).

The **Ľubietová - Svätodušná** Cu-Fe ore deposit is located 5 km east from the village of Ľubietová. The quartz-carbonate (siderite, calcite, ankerite) ore veins are hosted by Paleozoic gneisses and granite porphyry (Figure 2) and the primary Cu minerals are chalcopyrite and tetrahedrite-tennantite (Ilavský, 1994). Beside these two, the veins contain arsenopyrite, pyrite, barite and rare galena. In the cementation zone, cuprite and native copper were identified (Koděra, 1990). A wide range of secondary minerals are present, mostly Cu and Cu-As phases

(Table 1). Mining activity continued intermittently from the Bronze Age until the end of the 19th century.

Potential environmental risk at both studied sites includes elevated concentrations of Cu, As and Sb leaching out of waste rock into the surrounding soils, ground and surface waters (Andráš et al., 2008; Franková et al., 2012; Andráš et al. 2013). The pH values of surface waters in Špania Dolina - Piesky is at most sites in range of 6.5 - 7.8 and in Ľubietová - Svätodušná in range of 6.0-7.5 (Franková et al., 2012). The mine waste dumps in the study areas have been subjected to weathering under a humid temperate climate; the mean annual precipitation and temperature are 600 mm and 8 °C, respectively.

Materials and Methods

Sample collection

Weathered samples with tetrahedrite-tennantite solid solution (hereafter ttd-tnn) and other ore minerals were collected from abandoned waste rock piles from Špania Dolina - Piesky and Ľubietová - Svätodušná. At Špania Dolina - Piesky, some samples were collected directly from the oxidation zone *in situ*. Grain sizes of the waste material range from boulder-size fragments to fine-grained material. Samples were chosen based on the occurrence of visible oxidation products associated with relics of ttd-tnn grains and similarities in color and texture of completely altered samples with those oxidation products. Standard thin sections (30 μm thick) were prepared and inspected in transmitted and reflected polarized light.

Electron microprobe analysis (EPMA)

Electron microprobe analyses of primary minerals and their oxidation products were performed on a JEOL JXA-8230 electron microprobe in a wavelength-dispersive mode (WDS) under the conditions of 20 kV, 20 kV, 30 nA, and beam size of 1-6 μm at Queen's University, Kingston, Canada. Calibration was carried out using the following lines, standards, detector crystals and counting time on each peak and the same counting times for background: synthetic standards for As (Lα, $FeAs_2$, TAP, 60 s), Fe (Kα, $CuFeS_2$, LIFL, 20 s), Zn (Kα, ZnS, LIFL, 20 s), Bi (Lα, Bi metal, LIFL, 60 s), Cu (Kα, Cu_2S, LIF, 30 s), Ag (Lα, Ag metal, PETH, 60 s), Mg (Kα, $CaMgSi_2O_6$, TAP, 40 s), Ca (Kα, $CaMgSi_2O_6$, PETH, 20 s) and Si (Kα, $CaMgSi_2O_6$, TAP, 20 s) and natural tetrahedrite for Sb and S (Harvard, 3137x): Sb (Lα, PET, 40 s), S (Kα, PET, 20 s). The analytical results for ttd-tnn were recalculated on the basis of 29 atoms per formula unit (apfu).

Synchrotron micro-analysis

Thin sections were detached from the glass slides prior to synchrotron analyses and mounted on Kapton™. Micro-X-ray fluorescence spectroscopy (μXRF), micro-X-ray diffraction (μXRD) and micro-X-ray absorption near-edge structure spectroscopy (μ-XANES) analyses of ttd-ttn weathering products were collected at the undulator beamline 20-ID at the Advanced Photon Source (Argonne, IL, USA) using a monochromatic beam focused to 5×5 μm and 3×3 μm. Samples were oriented 45° to the beam. All Sb μ-XANES spectra were collected around the Sb *K*-edge (30 491 eV). XANES spectra of standards were collected from all samples using an unfocused beam, approximately 0.5 mm in diameter. Synthetic tripuhyite was synthesized following the method of Diemar (2008), natural stibnite (from the Beaver Brook antimony mine, Newfoundland) and Sb_2O_3 oxide senarmontite (obtained commercially from Fisher Scientific)

were verified by conventional powder XRD prior to the synchrotron micro-analysis. Conventional powder XRD analyses were carried out with a Philips X-Pert diffractometer at Queen's University, employing CuKα radiation and an Ni filter.

Prior to synchrotron analyses, the standards were ground, spread uniformly on a Kapton tape, and the tape was folded 10-12 times. A Si (311) double-crystal monochromator was used to control the X-ray energy and was calibrated with the Sb foil at the Sb *K*-edge. XANES spectra of the standards were collected in a transmission mode. Spectra from samples were collected in a fluorescence mode and three to five scans were collected for each standard and sample. XANES spectra were normalized, aligned, merged and fitted to model spectra using the linear combinations fitting (LCF) algorithm in the ATHENA software (Ravel and Newville, 2005). The μXRD data were acquired in a transmission mode at a constant energy of 31 keV with a MAR165 CCD detector with binning to 2048 x 2048 array and nominal 80 μm pixel size. Calibration of the CCD detector was done using a LaB_6 standard. Calibrations and corrections were done using Fit2D software (Hammersley, 1996). The phases were identified and structures were refined using HIGHSCORE PLUS software. The background parameters, specimen displacement, unit cell parameters and peak profile parameters were refined.

196 ## Results and Discussion

197

198 ### Chemical composition of primary tetrahedrite-tennantite minerals

199 The tetrahedrite-tennantite solid solution (ttd-tnn) in our samples from Špania Dolina - Piesky
200 contains Sb (up to 2.90 apfu), less As (up to 1.35 apfu) and a small amount of Bi (up to 0.12
201 apfu) (Table 2). Copper (up to 10.63 apfu) is the dominant cation in the trigonal site, and is
202 isomorphically substituted by Ag (up to 0.06 apfu). The tetrahedral position includes divalent
203 cations such as Zn (up to 0.45 apfu), Fe (up to 1.11 apfu) and since the Cu apfu value is higher
204 than 10, part of Cu is assumed to occupy the tetrahedral position. The measured composition of
205 the tetrahedrite agrees well with the microprobe data of the tetrahedrite ore from this locality
206 described by Sejkora et al. (2013). Chemical composition of the ttd-tnn from Ľubietová -
207 Svätodušná is more variable. The composition of tennantite is shown in Table 2. Tennantite
208 contains As with apfu value up to 3.05. Antimony content is up to 1.01 apfu and Bi has apfu
209 value up to 0.08. Zinc (apfu value up to 0.16) and Ag (apfu up to 0.33) were also detected.
210 Copper is dominant with apfu up to 10.15. High levels of Fe (up to 1.91 apfu) were measured.
211 Tetrahedrite samples from Ľubietová - Svätodušná contain Sb (2.08-2.85 apfu), As (0.92-1.29
212 apfu), Cu (1.15-13.45 apfu), Fe (1.06-1.32 apfu), Zn (0.12-0.20 apfu) and in some cases
213 increased amounts of Ag (maximum of 9.97 apfu).

214 ### Tetrahedrite weathering products

215 In the samples from Špania Dolina - Piesky, oxidation products formed by tetrahedrite
216 decomposition are represented by secondary phases dominated by Sb-Cu-As-Fe, commonly
217 associated with other supergene minerals like Cu arsenates, carbonates and sulfates. The
218 secondary Cu oxysalts from the upper part of the oxidation zone were described by Števko
219 (2014). In hand specimen, the oxidation products of tetrahedrite range in color from yellowish

green to dark olive green (Figure 3). Some of the samples contain relics of the primary tetrahedrite, other ones are completely altered with no remnants of the primary ore. When observed in a petrographic microscope, the oxidation products comprise green porous, spongy mass and brown thin veinlets that fill microscopic fractures between the former tetrahedrite grains. In the backscattered-electron (BSE) images, the veinlets appear brighter and the porous mass darker (Figure 4A). The veinlets are also present where no tetrahedrite relics are observed. The secondary phases in the veinlets were identified by μXRD as a mixture of tripuhyite $FeSbO_4$ and a roméite-group mineral or minerals. Smooth rings of μXRD patterns are suggestive of nanocrystalline nature of tripuhyite and roméite (Figure 4A, B; cf. Walker et al., 2005). The porous mass consists of X-ray amorphous Cu-As-Fe-Sb oxyhydroxides. These X-ray amorphous masses are sometimes intergrown with aggregates of nanocrystalline goethite and tripuhyite (Figure 4B).

X-ray amorphous oxidation products. The X-ray amorphous phases are olive-green in color in hand specimen and transmitted polarized light. Amorphous phases can be distinguished from the mixture of roméite and tripuhyite because this mixture is characterized by light brown color (probably caused by the presence of tripuhyite). The X-ray amorphous phases have the highest As content of all the studied tetrahedrite oxidation products, ranging from 10.58 wt% to 20.16 wt% (average of 17.13 wt%). Copper concentration in the X-ray amorphous masses is very high (average of 23.09 wt %). The content of Fe in the X-ray amorphous phases shows only slight variations (from 8.06 wt% to 10.56 wt%) (Table 3). The Sb/As ratio is variable. Based on Sb/As ratios we could define two trends. Most of the analyses belong to phases with lower Sb concentration ranging from 2.41 wt% to 4.49 wt %. As/Sb (R^2=0.58), As/Fe (R^2=0.42), As/Cu (R^2=0.45), Sb/Fe (R^2=0.44), Sb/Cu (R^2=0.50), Fe/Cu (R^2=0.21) show positive correlation

(Figure 5). These phases did not diffract under the conditions of the synchrotron-based μXRD experiments. The second group are phases characterized by higher Sb concentration ranging from 10.82 wt% to 19.44 wt%. The chemical composition of amorphous phases belonging to this group is similar in composition to roméite reported in this study. The μXRD patterns display one broad peak with low intensity corresponding to *d*-spacing between 2.91-3.02 Å, which agrees with the most intense diffraction peak characteristic for the roméite structure (Zedlitz, 1932). In this group, substitution of Sb for As, and Sb for Cu is suggested by the good negative correlation (Sb/(As+Cu), R^2= 0.81, Figure 6). Antimony was present as Sb^{5+} in X-ray amorphous phases produced by tetrahedrite weathering. Usually, the initial X-ray amorphous phases transform over time into more crystalline phases which are assumed to be more stable (Majzlan et al., 2007). We suggest that, in our samples, roméite results from such a transformation from an earlier X-ray amorphous phase. This is supported by observation of the X-ray amorphous phases being consistently associated with poorly crystalline roméite.

Roméite-group minerals and tripuhyite. In some analyses, roméite was the only crystalline phase identified by μXRD. It is not clear whether there is actually a mixture of X-ray amorphous phases and roméite and, if so, what is the proportion of Fe, As and Cu possibly hosted by the X-ray amorphous phase. Therefore, the following Wavelength dispersive spectroscopy analyses (WDS) could reflect chemical composition of pure roméite or roméite-X-ray amorphous phase mixture: As with minimal concentration of 7.92 wt%, maximum of 16.38 wt% (average of 15.22 wt%), Sb ranged from 10.42 wt% to 27.45 wt% (average of 16.55 wt%), Cu content varied from 11.62 wt % to 44.22 wt % (average of 25.58 wt%), Fe minimum content was 1.08 wt% and maximum of 12.67 wt% (average of 9.21 wt%; Table 4), range of Bi concentration was 0.88 wt% to 5.04 wt% (average of 2.82 %). The refined lattice parameter *a*

varied from 10.203(6) to 10.367(9) Å (Table 4). A negative Sb/Cu correlation (R^2 = 0.8) could reflect Cu being hosted by X-ray amorphous phases whereas Sb being present in roméite structure. Sb^{5+} has been reported to substitute for Fe^{3+} in pyrochlores (Atencio et al., 2010), however, we do not observe any significant negative Sb/Fe correlation (R^2 = 0.11) in our samples (Figure 6). We are not aware of a naturally occurring roméite with similar As content as that reported in this study. Christy and Gatedal (2005) described roméite from a skarn in Långban, Sweden, with As content up to 2.88 wt%. Based on the ionic radii of As^{3+} and As^{5+} of 0.50 Å and 0.47 Å, respectively, and the coordination with oxygen atoms, As is more likely to fit in the *A* position in the structure of pyrochlores. Arsenic oxidation state was not determined in our samples. Pyrochlore supergroup nomenclature is based on the ions occupancy of the *A*, *B* and *Y* sites. A proper name for the phase described in this study is debatable. Partzite (or cuproroméite) is a questionable Cu-dominant member of the roméite-group minerals from the pyrochlore supergroup. Ertl and Brandtatter (2000) identified "partzite", as a phase with a formula $(Cu^{+2},As^{+3},Fe^{+2},Zn^{+2})_2(Sb^{+5},Fe^{+3})_2O_6(O,OH,F)$ with the unit-cell parameter a = 10.295(10) Å. This material is a weathering product of tetrahedrite. Škácha et al. (2009) identified material with composition close to partzite in association with cuprostibite in mine dump of the Příbram uranium - base metal ore district in central Czech Republic and assigned a formula of $(Cu_{2.23}Pb_{0.01})_{\Sigma 2.24}$ $(Sb_{1.70}As_{0.01})_{\Sigma 1.71}O_6$. Further work is required to establish if a Cu-dominant roméite-group mineral really exists or not (Roper et al., 2012); as of now, such mineral is not approved by the IMA.

Tripuhyite was rarely found in our thin sections as a single phase; more common was a mixture with roméite, less common with goethite. The chemical composition of single tripuhyite was not determined for the samples in this study. Chemical composition of a nanocrystalline mixture of

tripuhyite with a roméite-group mineral indicated that As varied from 0.96 wt% to 14.51 wt% (average of 9.20 wt%), for Sb the minimum content was 2.27 wt% and maximum of 42.13 wt% % (average of 28.65 wt%), Cu ranged from 3.42 wt% up to 25.75 wt% (average of 15.10 wt%) and minimum value of Fe detected was 9.09 wt%, maximum 48.54 wt% (average of 13.36 wt%; Table 5). Lesser amounts of Bi (maximum of 2.36 wt%), Si (maximum of 1.26 wt%) and Ca (maximum of 4.36 wt%) were also present. The mass of tripuhyite in this mixture ranged from 35% to 47%. Good negative correlations of Sb/Fe (R^2=0.76), As/Sb (R^2=0.96) and Sb/Cu (R^2=0.91) were detected (Figure 6). Antimony and Fe in tripuhyite can be present in different ratios (Lalinská-Voleková et al., 2012). Variation in the calculated values of the unit-cell parameters for tripuhyite indicate different proportions of Sb/Fe and other elements (most likely As) entering its structure. The calculated unit cell parameters for tripuhyite are: a = 4.56(1) – 4.671(3) Å, c = 3.036(3) – 3.056(4) Å, V = 63.72 – 66.90 Å^3 (Table 5).

μ-XANES analysis indicates that Sb^{5+} is the dominant oxidation state of antimony in the tetrahedrite oxidation products. The statistical goodness of fit parameters obtained from the linear combination fitting method (LC) R-factor and χ^2 are shown in Table 6. Additionally, the goodness of fit can be evaluated from the difference between the experimental data and LC data plotted as a difference curve (Figure 7, A, B). LC fitting of the Sb XANES spectra was performed from 30 eV below the adsorption edge up to 100 eV over the absorption edge for the normalized derivative spectra. Fitted spectra showed the presence of Sb^{3+} (0 – 21 %) and Sb^{5+} (78 – 100%). We assume Sb^{3+} and Sb^{5+} are present in roméite and Sb^{5+} in tripuhyite. The best statistical data were obtained with the standards senarmontite (Sb^{3+}-O) together with tripuhyite (Sb^{5+}-O). μ-XRF has been employed to examine the elemental distribution in the tetrahedrite weathering products (Figure 8). If we compare the concentration for different

312 elements in the secondary phases, Sb is mostly hosted by tripuhyite and roméite, and different
313 Fe/Sb ratios correspond to this mixture. As is hosted mostly by the X-ray amorphous phases and
314 roméite and in these phases, Sb/As ratios scatter significantly (Figure 9). Roméite is the most
315 important Cu host.

316

317 **Chemical composition and mineralogy of tennantite oxidation products**

318 Oxidation products directly associated with tennantite from Ľubietová-Svätodušná are brown-
319 green in hand specimens and in transmitted light. In the BSE images, they appear as rims on
320 tennantite grains, as alteration products forming adjacent to the tennantite grains or as alteration
321 products without tennantite relics (Figure 10 A, B). Oxidation rims and alteration products
322 directly related to tennantite grains are X-ray amorphous with abundant As (average 20.6 wt%),
323 Cu (23.41 wt%) Fe (13.05 wt%) and relatively low Sb concentration (2.86 wt%; Table 7). Other
324 secondary Cu-bearing phases associated with tennantite weathering in these samples are
325 chrysocolla and cuprite. Arsenic is hosted by pharmacosiderite and scorodite. Low
326 concentrations of As (average 0.65 wt%), Cu (0.72 wt %) and Sb (0.15 wt%) were detected in
327 goethite grains. No tennantite relics were observed associated with these crystalline phases.

328

329 **Implications**

330 Characterization of weathered and partially dissolved minerals at the microscale allowed insight
331 into the source of leachable metal(oid)s from the dumps of the waste rocks. The oxidation and
332 decomposition of the ttd-tnn minerals results in the formation of various secondary phases and
333 drives the release or retention of the elements in the near-surface oxidizing and wet environment.
334 Tetrahedrite oxidation products from Špania Dolina - Piesky contain significant amounts of
335 potentially toxic elements, mostly Sb, As and Cu. Antimony, As and Cu in these oxidation
336 products are hosted differently: Sb concentration is highest in analytical spots identified as
337 tripuhyite and roméite, As and Cu are preferentially hosted by X-ray amorphous phases and
338 roméite. Antimony is less mobile compared to elements like As, S and Cu, which are largely
339 present as supergene minerals (e.g. antlerite, azurite, brochantite, chalcophyllite, clinoclase,

cornwallite or malachite) at the localities and where the primary source is tetrahedrite and Sb concentration is high enough for Sb secondary minerals to be supersaturated. Elevated Sb concentrations in the adjacent streams (Franková et al., 2012) are likely related to the oxidation of tetrahedrite although the exact mechanisms controlling the release and attenuation of Sb have not yet been determined. If the primary Sb source is close to tennantite composition, Sb enters X-ray amorphous phases.

Acknowledgements

This research used resources of the Advanced Photon Source, a U.S. Department of Energy (DOE) Office of Science User Facility operated for the DOE Office of Science by Argonne National Laboratory under Contract No. DE-AC02-06CH11357. Data were collected at the X-ray Operations and Research beamline 20-ID-C. The authors would like to thank Robert Gordon and Zou Finfrock for providing beamline assistance at PNC/XOR and Brian Joy of Queen's University for EPMA technical assistance. This study was supported by the Slovak Research and Development Agency under the contract No. APVV-0663-10: “Contamination of mining country by toxic elements at selected Cu-deposits and possibilities of its remediation" and by a Natural Science and Engineering Research Council of Canada Discovery Grant to Heather Jamieson.

References cited

Andráš, P., Lichý, A., Rusková, J., and Matúšková, L. (2008) Heavy metal contamination of the landscape Ľubietová deposit (Slovakia). Proceedings of World Academy of Science, Engineering and Technology, 34, ISSN 2070 – 3740, Venice, Italy, 97-100.

Andráš, P., Dirner, V., Kharbish, S., and Krnáč, J. (2013) Characteristics of heavy metal distribution at spoil dump-fields of Cu deposit Lubietova (Slovakia), Carpathian Journal of Earth and Environmental Sciences, 8, 87 – 96.

Arlt, T., and Diamond, L. W. (1998) Composition of tetrahedrite-tennantite and "schwazite" in the Schwaz silver mines, North Tyrol, Austria. Mineralogical Magazine, 62, 801–820.

Atencio, D., Andrade, M.B., Christy, A. G., Giere, R., and Kartashov, P.M. (2010) The Pyrochlore Supergroup of Minerals: Nomenclature. Canadian Mineralogist, 48, 673–698.

Baláž, P. (2000) Extractive Metallurgy of Activated Minerals, 277p. Elsevier, Amsterdam.

Berlepsch, P., Armbruster, T., Brugger, J., Criddle, A. J., and Graeser, S. (2003) Tripuhyite, $FeSbO_4$ - revisited. Mineralogical Magazine, 67, 31–46.

Bolanz, R.M., Bläß, U., Ackermann, S., Ciobota, V., Rösch, P., Tarcea, N., Popp, J., and Majzlan, J. (2013) The effect of antimonate, arsenate and phosphate on the transformation of ferrihydrite to goethite, hematite, feroxyhyte, and tripuhyite. Clays and Clay Minerals, 61, 11-25,

Bowell, R.J. (1994) Sorption of arsenic by iron oxides and oxyhydroxides in soils. Applied Geochemistry, 9, 279-286.

377 Christy, A.G., and Gatedal, K. (2005) Extremely Pb-rich rock-forming silicates including a
378 beryllian scapolite and associated minerals in a skarn from Långban, Värmland,
379 Sweden. Mineralogical Magazine, 69, 995-1018.

380 Čillík I., Kusein M., Makuša M., Šuchová M., Tupý P., Valko P., and Dvoršťák J. (1986) Final
381 report Glezúr-Piesky, Špania Dolina-Mária adit 31.12.1986. 136p. ŠGÚDŠ-Geofond, Bratislava,
382 (in Slovak).

383 Courtin-Nomade, A., Rakotoarisoa, O., Bril, H., Grybos, M., Forestier, L., Foucher, F., and
384 Kunz, M. (2012) Weathering of Sb-rich mining and smelting residues: Insight in solid speciation
385 and soil bacteria toxicity. Chemie der Erde - Geochemistry, 72, 29–39.

386 DeSisto, S.L., Jamieson, H.E., and Parsons, M.B. (2011) Influence of hardpan layers on arsenic
387 mobility in historical gold mine tailings. Applied Geochemistry, 26, 2004-2018.

388 Diemar, G.A. (2008) Supergene dispersion of antimony and geochemical exploration model for
389 antimony ore deposits, 70 p. Ph.D. thesis. University of Western Sydney.

390 Diemar G. A., Filella M., Leverett P., and Williams P. A. (2009) Dispersion of antimony from
391 oxidizing ore deposits. Pure and Applied Chemistry, 81, 1547–1553.

392 Ertl, A., and Brandstätter, F. (2000) Protopartzite or thrombolite from magnesite quarry Veitsch,
393 Sattlerkogel, Styria, Austria. Joannea-Mineralogie, 1, 27–30 (in German).

394 Figuschová, M. (1977a) Secondary copper minerals from Špania Dolina. In: Hornická Příbram
395 ve vědě a technice - sekce mineralogie rudných ložisek, 55-70 (in Slovak).

396 Figuschová M. (1977b) Secondary copper minerals from Ľubietová. In: Zborník referátov z
397 konferencie Ložiskotvorné procesy Západných Karpát, Bratislava, 134-137 (in Slovak).

398 Filella, M.,Williams, P.A., and Belzile, N. (2009) Antimony in the environment: knowns and
399 unknowns. Environmental Chemistry, 6, 95–105.

400 Filippou, D., St-Germain, P., and Grammatikopoulos, T. (2007) Recovery of metal values from
401 copper-arsenic minerals and other related resources. Mineral Processing and Extractive
402 Metallurgy Review, 28, 247-298.

403 Flemming, R.L., Salzsauler, K., Sherriff, B.L., and Sidenko, N. (2005) Identification of scorodite
404 in very fine-grained, high-sulfide arsenopyrite mine wastes using Micro X-ray diffraction
405 (μXRD). Canadian Mineralogist, 43, 1527-1537.

406 Franková, H., Čmielová, L., Klimko, T., Lacková, E., and Andráš, P. (2012) Comparative study
407 of Cu, As and Sb toxicity between dump-fields of abandoned Cu-deposits Ľubietová and Špania
408 Dolina (Central Slovakia). Carpathian Journal of Earth and Environmental Sciences, 4, 79-88.

409 Hammersley, A.P., Svensson, S.O., Hanfland, M., Fitch, A.N., and Hausermann, D. (1996) Two-
410 dimensional detector software: From real detector to idealized image or two-theta scan. High
411 Pressure Research, 14, 235–248.

412 Harris, D.L., Lottermoser, B.G., and Duchesne, J. (2003). Ephemeral acid mine drainage at the
413 Montalbion silver mine, north Queensland. Australian Journal of Earth Sciences, 50, 797–809.

414 Hiller, E., Petrák, M., Tóth, R., Lalinská-Voleková, B., Jurkovič, Ľ., Kučerová, G., Radková A.,
415 Šottník, P., and Vozár, J. (2013) Geochemical and mineralogical characterization of a neutral,

low-sulfide/high-carbonate tailings impoundment, Markušovce, eastern Slovakia. Environmental Science and Pollution Research, 20, 7627–7642.

Ilavský, J., Vozárová, A., and Vozár, J. (1994) Ľubietová – exploration boreholes: Lu-1, Lu-2 a Lu-3. 77p. ŠGÚDŠ-Geofond, Bratislava (in Slovak).

Johnson, N. E., Craig, J. R., and Rimstidt, J. D. (1986) Compositional trends in tetrahedrite. Canadian Mineralogist, 397, 385–397.

King, R.J. (2001) The tetrahedrite group. Geology Today, 17, 77-80.

Klimko, T., Lalinská, B., Majzlan, J., Chovan, M., Kučerová, G., and Paul, C. (2011) Chemical composition of weathering products in neutral and acidic mine tailings from stibnite exploitation in Slovakia. Journal of GEOsciences, 6, 327–340.

Koděra, M., Andrusovová-Vlčeková, G., Belešová, O., Briatková, D., Dávidová, Š., Fejdiová, V., Hurai, V., Chovan, M., Nelišerová, E., and Ženiš, P. (1990) Topographic Mineralogy of Slovakia, Volume 3. Veda (in Slovak).

Kusein, M., and Maťová, V. (2002) Final report: Complex evaluation of closed deposit Špania Dolina. 172p. ŠGÚDŠ-Geofond, Bratislava (in Slovak).

Lalinská-Voleková, B., Majzlan, J., Klimko, T., Chovan, M., Kučerová, G., Michňová, J., Hovorič, R., Gottlicher, J., and Steininger, R. (2012) Mineralogy of weathering products of Fe-As-Sb mine wastes and soils at several Sb deposits in Slovakia. Canadian Mineralogist, 50, 481 – 500.

435 Lengke, M. F., Sanpawanitchakit, C., and Tempel, R. N. (2009) The oxidation and dissolution of
436 arsenic-bearing sulfides. Canadian Mineralogist, 47, 593–613.

437 Leverett, P., Reynolds, J.K., Roper, A.J., and Williams, P.A. (2012) Tripuhyite and schafarzikite:
438 Two of the ultimate sinks for antimony in the natural environment. Mineralogical Magazine, 76,
439 891–902.

440 Lynch, J. (1989) Large-scale hydrothermal zoning reflected in the tetrahedrite-freibergite solid
441 solution, Keno Hill Ag-Pb-Zn district, Yukon. Canadian Mineralogist, 27, 383–400.

442 Majzlan, J., Lalinská, Chovan, M., B., Jurkovič, L., Milovská, S., and Göttlicher, J. (2007) The
443 formation, structure, and ageing of As-rich hydrous ferric oxide at the abandoned Sb deposit
444 Pezinok (Slovakia). Geochimica et Cosmochimica Acta, 71, 4206-4220.

445 Majzlan, J., Lalinská, B., Chovan, M., Bläß, U., Brecht, B., Göttlicher, J., Steininger, R., Hug,
446 K., Ziegler, S., and Gescher, J. (2011) A mineralogical, geochemical, and microbiogical
447 assessment of the antimony- and arsenic-rich neutral mine drainage tailings near Pezinok,
448 Slovakia. American Mineralogist, 96, 1-13.

449 Michňová J., and Ozdín D. (2010) Genetic study of the primary hydrothermal mineralization in
450 Špania Dolina and Ľubietová ore districts (Slovakia, Western Carpathians). Mineralogica et
451 Petrographica Acta, 6, 237.

452 Moëlo, Y., Makovicky, E., Mozgova, N.N., Jambor, J.L., Cook, N., Pring, A., Paar, W., Nickel,
453 E.H., Graeser, S., Karup-Møller, and others (2008) Sulfosalt systematics: a review. Report of the
454 sulfosalt sub-committee of the IMA Commission on Ore Mineralogy, 7–46.

455 Moldovan, B.J., and Hendry, M.J. (2005) Characterizing and quantifying controls on arsenic
456 solubility over a pH range of 1–11 in a uranium mill-scale experiment. Environmental Science &
457 Technology, 37, 873–879.

458 Nickel, E.H. (1984) The mineralogy and geochemistry of the weathering profile of the
459 Teutonic Bore Cu-Pb-Zn-Ag sulphide deposit. Journal of Geochemical Exploration, 22,
460 239-264.

461 Nordstrom, K.D., Majzlan, J., and Königsberger, E. (2014) Thermodynamic Properties
462 for Arsenic Minerals and Aqueous Species. Reviews in Mineralogy & Geochemistry, 79,
463 217-255.

464 Novotný J. (1960) Mineralogical and Geochemical assessment of locality Špania Dolina-
465 Piesky. 145p. ŠGÚDŠ-Geofond, Bratislava (in Slovak).

466 Pauliš P. (1981) Chalcophyllite occurrence at Ľubietová-Svätodušná. Časopis pro Mineralogii
467 a Geologii, 26, 213 (in Czech).

468 Polák M., Filo I., Havrila M., Bezák V., Kohút M., Kováč P., Vozár J., Mello J., Maglay J.,
469 Elečko M., and others (2003) Geological map of Starohorské mountains, Čierťaž and the
470 northern part of Zvolenská valley. 1:50 000. ŠGÚDŠ-Geofond, Bratislava (in Slovak).

471 Ravel, B., and Newville, M. (2005) ATHENA, ARTEMIS, HEPHAESTUS: data analysis for X-
472 ray absorption spectroscopy using IFEFFIT. Journal of Synchrotron Radiation, 12, 537–541.

473 Regásek F. (1973) Mineralogical and Geochemical study of sulfidic mineralization at Piesky
474 (Špania Dolina). 10p. ŠGÚDŠ-Geofond, Bratislava, (in Slovak).

Ritchie, V. J., Ilgen, A. G., Mueller, S. H., Trainor, T. P., and Goldfarb, R. J. (2013). Mobility and chemical fate of antimony and arsenic in historic mining environments of the Kantishna Hills district, Denali National Park and Preserve, Alaska. Chemical Geology, 335, 172–188.

Řídkošil, T. (1978) Secondary copper minerals, Špania Dolina-Piesky, Slovakia. Časopis pro Mineralogii a Geologii, 23, 436-437 (in Czech).

Řídkošil T., and Medek Z. (1981) New findings from Svätodušná (central Slovakia). Časopis pro mineralogii a geologii, 26, 1, 91 (in Czech).

Řídkošil, T., and Povondra, P. (1982) New data about antlerite from Špania Dolina-Piesky, Slovakia. Časopis pro Mineralogii a Geologii, 27, 79-84 (in Czech).

Řídkošil T. (2007) Secondary copper minerals from Ľubietová, Slovakia. Minerál, 15, 433-437 (in Czech).

Roper, A.J., Williams, P.A., and Filella, M. (2012) Secondary antimony minerals: Phases that control the dispersion of antimony in the supergene zone. Chemie der Erde - Geochemistry, 72, 9–14.

Roper, A.J., Leverett, P., Murphy, T.D., and Williams, P.A. (2015) Stabilities of byströmite, $MgSb_2O_6$, ordoñezite, $ZnSb_2O_6$ and rosiaite, $PbSb_2O_6$, and their possible roles in limiting antimony mobility in the supergene zone. Mineralogical Magazine, 79, 537-544.

Rusínová, P., Kučerová, G., and Lalinská-Voleková B. (2014) Mineralogical study of synthetic and natural tripuhyite $FeSbO_4$. Proceedings of the international symposium CEMC 2014, p. 126-127. Masaryk University, Brno, Czech Republic.

Sejkora, J., Števko, M., and Macek, I. (2013) Contribution to chemical composition of tetrahedrite from the Piesky copper deposit, the Špania Dolina ore district, central Slovakia. Bulletin mineralogicko-petrologického oddělení Národního muzea (Praha), 21, 89-103.

Škácha P., Sejkora J., Litochleb J., and Hofman P. (2009) The occurrence of cuprostibite in the Příbram uranium-base metals ore district (the shaft 16, Příbram - Háje), Czech Republic. Bulletin Mineralogicko-petrografického oddělení Národního muzea v Praze, 17, 73-78 (in Czech).

Števko, M., and Sejkora, J. (2012) Supergene arsenates of copper from the Piesky deposit, Špania Dolina, Central Slovakia. Acta Mineralogica Petrographica, 7, 130.

Števko, M. (2014) Mineralogical characterization of supergene copper arsenates from the Novoveská Huta, Poniky and Špania Dolina localities. 189 pp. Ph.D. thesis, Comenius University, Bratislava (in Slovak).

Vassileva, R. D., Atanassova, R., and Kouzmanov, K. (2014) Tennantite-tetrahedrite series from the Madan Pb-Zn deposits, Central Rhodopes, Bulgaria. Mineralogy and Petrology, 108, 515–531.

Vozárová, A., Konečný, P., Vďačný, M., Vozár, J., and Šarinová, K. (2014) Provenance of Permian Malužiná Formation sandstones (Hronicum, Western Carpathians): evidence from monazite geochronology. Geologica Carpathica 65, 329-338.

Walker, S. R., Parsons, M.B., Jamieson, H., and Lanzirotti, A. (2009) Arsenic mineralogy of near-surface tailings and soils: Influences on arsenic mobility and bioaccessibility in the Nova Scotia gold mining districts, Canadian Mineralogist, 47, 533–556.

Walker S. R., Jamieson H. E., Lanzirotti A., Andrade C. F., and Hall G. E. M. (2005) The speciation of arsenic in iron oxides in mine wastes from the Giant gold mine, N.W.T.: Application of synchrotron micro-XRD and micro-XANES at the grain scale. Canadian Mineralogist, 43, 1205–1224.

Wilson, N.J, Craw, D., and Hunter, K. (2004) Antimony distribution and environmental mobility at an historic antimony smelter site, New Zealand. Environmental Pollution, 129, 257-266.

Žebrák P. (1986) Prehistorical copper mining, Špania Dolina-Piesky. AVANS, 256-257 (in Czech).

Zedlitz, O. (1932) Die Kristallstruktur von Romeit und Schneebergit. Zeitschrift für Kristallographie, 81, 253-263 (in German).

Figure 1. Generalized geological map and a photograph of waste rock pile of Špania Dolina area, showing the location of the historical waste rock piles with bedrock geology simplified from Polák et al. (2003). 1 – Variscan basement (orthogneiss and amphibolite) 2- Paleozoic (conglomerate, arcose, greywacke) 3- Cretaceous (limestone and dolomite) 4 - Jurassic (chert, sandstone and limestone) 5 - Triassic (quartzite, dolomite, limestone) 6- faults, 7-thrust faults, 8-waste rock piles, 9- streams

Figure 2. Geological map of Ľubietová area simplified from Polák et al. (2003) Paleozoic: 1-gneiss and granite porphyry, 2- amphibolite, 3- metasandstone, meta-arcose, metaconglomerate, Mesosoic: 4 – dolomite, Tertiary: 5 – tuff, volcanic breccia conglomerate, 6 – Quaternary sediments, 7 – mineralization and waste rock piles, 8 – fault

Figure 3. Olive-green masses of oxidation products with relics of the primary tetrahedritefrom the oxidation zone of Špania Dolina-Piesky deposit.

Figure 4. BSE images of tetrahedrite weathering products A: an altered tetrahedrite (ttd) relic in a mixture of tripuhyite and roméite (spot1, μXRD – roméite-black, tripuhyite red) and X-ray amorphous Cu-As-Fe Sb phases; B: alteration products of tetrahedrite: spot2: poorly crystalline roméite, spot3: mixture of goethite and tripuhyite (μXRD-goethite-black, tripuhyite-red).

Figure 5. Elements variations in X-ray amorphous phases resulting from tetrahedrite weathering (all values are in wt% of elements).

Figure 6. Element variations in amorphous phases chemically similar to roméite, pure roméite and a nanocrystalline mixture of tripuhyite and roméite. All values are in wt% elements.

Figure 7. A: Sb XANES spectra of the model compounds and of the tripuhyite-roméite mixture (LCF: 84% Sb V and 16% Sb III-O, Analysis 1 in Table 6). B: An example of a LC fit of experimental data of tripuhyite-roméite mixture.

Figure 8. Distribution of Sb, As, Cu and Fe in the ttd oxidation products. Each row present a BSE image (left) and μXRF maps (collected at 31 keV) of the oxidation products.

Figure 9. Sb-As-Fe plot of the secondary minerals identified. All data from electron microprobe analyses.

Figure 10. BSE image of tennantite and X-ray amorphous oxidation products (light gray). A: tennantite grains showing advanced stages of weathering; B: oxidation rim on a tnn grain.

Table 1. The most common secondary minerals and their formulae described from the oxidation zone of Špania Dolina-Piesky deposit (Figuschová, 1997a; Řídkošil, 1978; Řídkošil and Povondra, 1982; Števko and Sejkora, 2012; Števko, 2014 and references therein) and Ľubietová-Svätodušná (Figuschová, 1977b; Řídkošil and Medek, 1981; Pauliš, 1981; Řídkošil, 2007)

Mineral name	Formula	Occurrence	
		Špania Dolina - Piesky	Ľubietová - Svätodušná
Antlerite	$Cu_3(SO_4)(OH)_4$	*	*
Azurite	$Cu_3(CO_3)_2(OH)_2$	*	*
Barite	$BaSO_4$	*	
Brochantite	$Cu_4SO_4(OH)_6$	*	*
Chalcophyllite	$Cu_{18}Al_2(AsO_4)_4(SO_4)_3(OH)_{24}\cdot 36H_2O$	*	*
Clinoclase	$Cu_3AsO_4(OH)_3$	*	*
Cornubite	$Cu_5(AsO_4)_2(OH)_4$		*
Cornwallite	$Cu_5(AsO_4)_2(OH)_4$	*	*
Cuprite	Cu_2O	*	*
Devilline	$CaCu_4(SO_4)_2(OH)_6\cdot 3H_2O$	*	
Euchroite	$Cu_2(AsO_4)(OH)\cdot 3H_2O$		*
Langite	$Cu_4SO_4(OH)_6\cdot 2H_2O$	*	*
Malachite	$Cu_2CO_3(OH)_2$	*	*
Olivenite	$Cu_2(AsO_4)(OH)$		*
Parnauite	$Cu_9(AsO_4)_2(SO_4)(OH)_{10}\cdot 7H_2O$		*
Bariopharmacosiderite	$BaFe_4(AsO_4)_3(OH)_5\cdot 5H_2O$	*	*
Posnjakite	$Cu_4SO_4(OH)_6\cdot H_2O$	*	
Pseudomalachite	$Cu_5(PO_4)_2(OH)_4$	*	
Posnjakite	$Cu_4SO_4(OH)_6\cdot H_2O$	*	
Scorodite	$FeAsO_4\cdot 2H_2O$		*
Strashimirite	$Cu_8(AsO_4)_4(OH)_4\cdot 5H_2O$		*

560 Table 2. Selected electron microprobe analyses of tetrahedrite grains form locality Špania Dolina Piesky and tennantite grains form locality
561 Ľubietová Svätodušná (8 representative analyses for each locality).

	Špania Dolina-Piesky									Ľubietová-Svätodušná									
wt%	**Cu**	**Ag**	**Fe**	**Zn**	**As**	**Sb**	**Bi**	**S**	**Total**	**wt%**	**Cu**	**Ag**	**Fe**	**Zn**	**As**	**Sb**	**Bi**	**S**	**Total**
1	42.37	0.12	3.95	1.23	6.11	20.22	0.68	26.5	101.18	1	40.17	2.03	6.79	0.67	14.52	7.07	1.01	26.94	99.2
2	42.16	0.12	3.81	1.27	5.32	21.41	0.65	26.2	100.95	2	41.74	0.99	6.88	0.63	14.56	7.1	1.04	27.21	100.15
3	41.59	0.13	3.87	1.27	5.04	21.79	0.75	26.21	100.65	3	40.56	1.86	6.81	0.64	14.56	7.04	0.94	26.85	99.27
4	42.45	0.11	3.92	1.18	6.38	20.05	0.75	26.42	101.25	4	41.44	1.23	6.91	0.66	13.86	8.07	1.14	27.13	100.44
5	41.34	0.14	3.87	1.22	5.97	20.23	0.63	26.33	99.73	5	42.52	0.51	6.86	0.61	14.37	7.26	0.88	27.28	100.29
6	41.97	0.14	3.79	1.21	4.53	22.01	0.82	26.09	100.56	6	42.35	0.67	6.91	0.59	14.32	7.37	0.91	27.27	100.4
7	42.24	0.13	3.87	1.16	5.68	20.14	0.55	26.32	100.09	7	42.24	0.6	6.85	0.67	14.85	7.44	0.89	27.05	100.59
8	42.18	0.13	3.86	1.19	5.45	20.58	0.82	26.07	100.28	8	41.78	0.81	6.77	0.62	14.95	7.19	0.87	26.82	99.81
apfu										**apfu**									
1	10.54	0.02	1.11	0.29	1.28	2.62	0.05	13.06		1	9.75	0.29	1.88	0.16	2.99	0.9	0.07	12.96	
2	10.57	0.02	1.09	0.31	1.13	2.8	0.05	13.02		2	10	0.14	1.88	0.15	2.96	0.89	0.08	12.92	
3	10.48	0.02	1.11	0.29	1.08	2.87	0.06	13.09		3	9.84	0.27	1.88	0.15	3.00	0.89	0.07	12.91	
4	10.56	0.02	1.11	0.28	1.35	2.6	0.06	13.02		4	9.95	0.17	1.89	0.15	2.82	1.01	0.08	12.91	
5	10.42	0.02	1.11	0.3	1.28	2.66	0.05	13.16		5	10.15	0.07	1.86	0.14	2.91	0.9	0.06	12.9	
6	10.6	0.02	1.09	0.3	0.97	2.90	0.06	13.06		6	10.11	0.09	1.88	0.14	2.9	0.92	0.07	12.9	
7	10.61	0.02	1.11	0.28	1.21	2.64	0.04	13.1		7	10.09	0.08	1.86	0.16	3.01	0.93	0.06	12.81	
8	10.63	0.02	1.11	0.29	1.16	2.71	0.06	13.02		8	10.06	0.12	1.86	0.14	3.05	0.9	0.06	12.8	

562

563

564 Table 3. Representative electron microprobe analyses of X-ray amorphous phases associated with tetrahedrite weathering (b.d.=below
565 the detection limit).

	As_2O_5	CuO	Fe_2O_3	Sb_2O_5	Bi_2O_3	Ag_2O	HgO	PbO	SO_3	Total
1	27.59	27.89	13.77	3.55	4.71	0.01	0.03	0.02	0.04	77.61
2	27.65	28.92	12.82	3.44	2.02	0.01	b.d.	b.d.	0.05	74.91
3	28.86	30.69	13.93	3.74	3.67	0.01	0.02	0.05	0.05	81.02
4	26.75	27.86	14.31	3.67	3.05	0.04	0.01	0.04	0.07	75.8
5	29.34	32.11	14.31	4.20	2.98	0.01	b.d.	b.d.	0.06	83.01
6	25.70	18.67	12.8	3.30	1.92	0.02	0.07	0.02	0.04	62.54
7	26.57	22.02	13.01	3.26	2.29	0.01	b.d.	b.d.	0.06	67.22
8	26.23	30.22	12.78	3.77	2.50	b.d.	b.d.	0.05	0.01	75.56
9	27.12	31.52	14.4	3.74	3.51	0.04	0.12	0.05	0.02	80.52
10	30.93	31.61	14.55	4.63	3.58	0.01	0.09	0.01	0.09	85.5

566

567

568 Table 4. Selected electron microprobe analyses and refined *a* unit cell parameter (synchrotron μXRD)- for roméite, possibly in a
569 mixture with the X-ray amorphous phases.

570

	As_2O_5	CuO	Fe_2O_3	Sb_2O_5	Bi_2O_3	Ag_2O	HgO	PbO	CdO	ZnO	SeO_2	SO_3	Total	*a* (Å)
1	24.55	33.74	14.08	18.22	4.31	0.19	0.01	0.05	0.07	0.03	0.24	0.14	95.63	10. 331(9)
2	21.49	29.81	11.99	27.26	4.66	0.10	0.00	0.00	0.08	0.08	b.d.	0.09	95.56	10.327(9)
3	25.13	33.21	14.84	19.64	3.12	0.05	0.05	b.d.	b.d.	0.06	b.d.	0.06	96.16	10.357(9)
4	17.24	27.89	11.47	31.84	4.18	0.14	0.08	0.07	0.05	0.04	b.d.	0.10	93.10	10.35(2)
5	22.03	31.69	12.01	26.18	3.86	0.13	0.00	0.05	0.12	0.02	b.d.	0.08	96.17	10.322(4)
6	23.89	31.99	13.61	17.92	3.62	0.21	0.05	0.01	0.08	0.04	0.11	0.16	91.69	10.35(1)
7	24.38	34.68	13.16	21.29	2.14	0.03	0.14	0.09	0.04	0.06	b.d.	0.08	96.09	10.35(1)
8	23.73	31.79	16.39	20.49	2.56	0.01	0.04	0.07	b.d.	0.06	b.d.	0.09	95.23	10.31(1)
9	15.62	40.75	10.51	20.54	0.98	1.57	0.28	0.02	0.01	0.02	0.24	0.57	91.11	10.28(1)

571

572

573 Table 5. Chemical composition of tripuhyite and roméite mixture (wt%) and refined unit cell parameters (synchrotron μXRD) for the
574 two minerals. * The mass balance calculation: Roméite formula was calculated from EMPA analyses for single roméite phase based
575 on 7 oxygens; in the mixture of tripuhyite and roméite all As and Cu are assumed to be hosted by roméite.
576

														Tripuhyite		Roméite	Mass balance	
	As_2O_5	CuO	Fe_2O_3	Sb_2O_5	Bi_2O_3	Ag_2O	HgO	PbO	CdO	ZnO	SeO_2	SO_3	Total	a/ Å	c/ Å	a/ Å	Tripuhyite %	Roméite %
1	6.96	9.99	15.00	54.34	2.64	b.d.	b.d.	0.01	0.05	0.07	b.d.	0.12	89.18	4.56(1)	3.13(2)	10.235(8)	43	57
2	6.94	9.85	16.13	52.74	0.21	0.01	0.08	0.00	0.11	0.06	b.d.	0.03	86.16	4.671(3)	3.036(3)	10.261(4)	44	56
3	7.36	10.15	17.90	51.09	1.07	b.d.	0.02	0.14	0.02	0.05	0.24	0.03	88.07	4.611(8)	3.087(9)	10.28(1)	43	57
4	6.48	10.21	15.91	53.05	b.d.	0.03	0.05	b.d.	0.07	0.04	0.14	0.10	86.08	4.591(8)	3.09(1)	10.266(8)	43	57
5	5.65	8.88	14.37	55.82	1.57	0.04	0.03	0.02	0.13	0.07	b.d.	0.05	86.63	4.586(9)	3.16(1)	10.33(1)	48	52
6	8.06	11.39	18.43	50.65	1.54	0.04	b.d.	0.03	b.d.	0.04	0.05	0.13	90.36	4.59(1)	3.09(2)	10.267(8)	40	60
7	6.60	9.57	14.38	55.48	0.54	0.01	0.03	b.d.	b.d.	0.05	0.25	0.03	86.94	4.55(2)	3.13(2)	10.269(8)	45	55
8	6.07	9.30	13.74	55.97	0.41	0.04	0.02	b.d.	0.07	0.06	0.17	b.d.	85.85	4.573(9)	3.19(1)	10.308(5)	46	54
9	10.34	14.46	24.18	42.77	0.89	0.01	0.01	0.04	0.05	0.08	0.06	0.06	92.95	4.586(2)	3.049(3)	10.201(5)	32	68

577

578

579 Table 6. Results of the LC fits of Sb XANES spectra for the tripuhyite-roméite mixtures resulting from tetrahedrite weathering
580 (analyses 1-6) together with statistical evaluation of goodness of fits. Sum of the components was normalized to 100%.

Analysis	Tripuhyite (Sb^{5+}- O) %	Sb_2O_3 (Sb^{3+}- O)%	R-factor	Chi-square
1	84	16	0.028272	0.00533
2	88	12	0.004928	0.0009
3	90	10	0.005666	0.00102
4	88	12	0.004495	0.00082
5	100	0	0.053702	0.00922
6	79	21	0.040014	0.0063

581

582

This is a preprint, the final version is subject to change, of the American Mineralogist (MSA)
Cite as Authors (Year) Title. American Mineralogist, in press.
(DOI will not work until issue is live.) DOI: http://dx.doi.org/10.2138/am-2017-5616

583 Table 7. Chemical composition of X-ray amorphous oxidation products associated with tennantite relics (wt%).

	As_2O_5	SiO_2	Fe_2O_3	ZnO	Bi_2O_3	CuO	SO_3	Sb_2O_5	MgO	CaO	Ag_2O	Total
1	31.04	0.24	14.91	0.06	2.14	34.28	0.36	5.69	0.02	0.13	0.06	88.93
2	31.01	0.27	16.28	0.06	2.15	32.66	0.45	5.74	0.03	0.15	0.03	88.83
3	27.68	0.27	15.16	0.09	1.94	33.69	0.42	5.54	0.03	0.15	0.09	85.06
4	27.74	0.27	12.11	0.09	1.67	39.96	0.55	6.13	0.00	0.07	0.06	88.65
5	29.86	0.25	13.29	0.13	2.06	36.95	0.49	5.86	0.01	0.07	0.00	88.97
6	26.17	0.35	12.26	0.16	1.54	42.97	1.27	6.33	0.03	0.16	0.02	91.26
7	30.41	0.08	14.09	0.07	1.56	35.73	1.90	1.09	0.00	0.15	4.79	89.87
8	30.35	0.17	16.75	0.08	1.97	34.29	0.61	4.69	0.00	0.11	0.03	89.05

584

585

This is a preprint, the final version is subject to change, of the American Mineralogist (MSA)
Cite as Authors (Year) Title. American Mineralogist, in press.
(DOI will not work until issue is live.) DOI: http://dx.doi.org/10.2138/am-2017-5616

586 Figure 1:

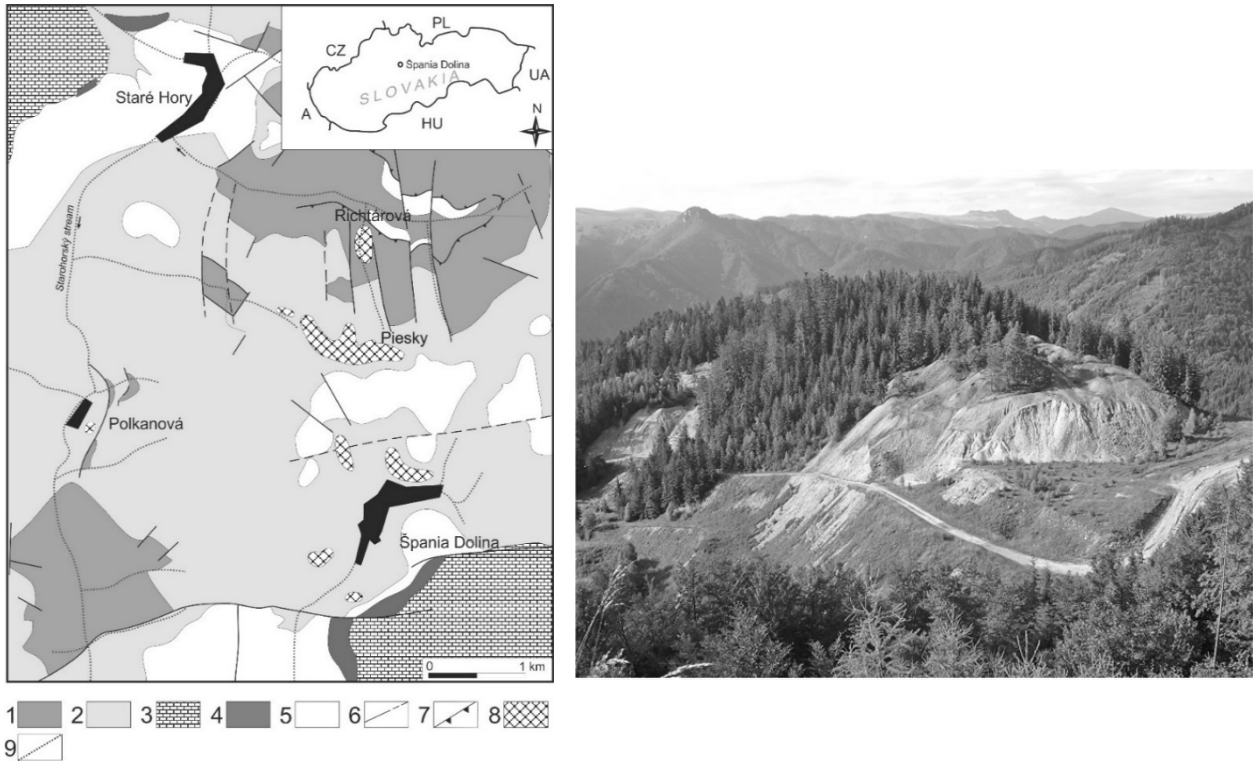

587

588

589

590 Figure 2

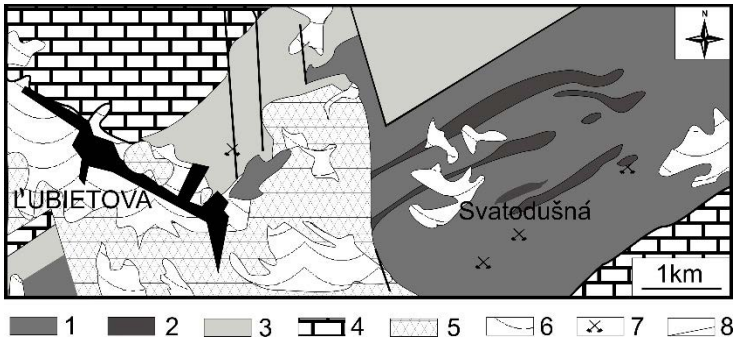

591

592

593 Figure 3:

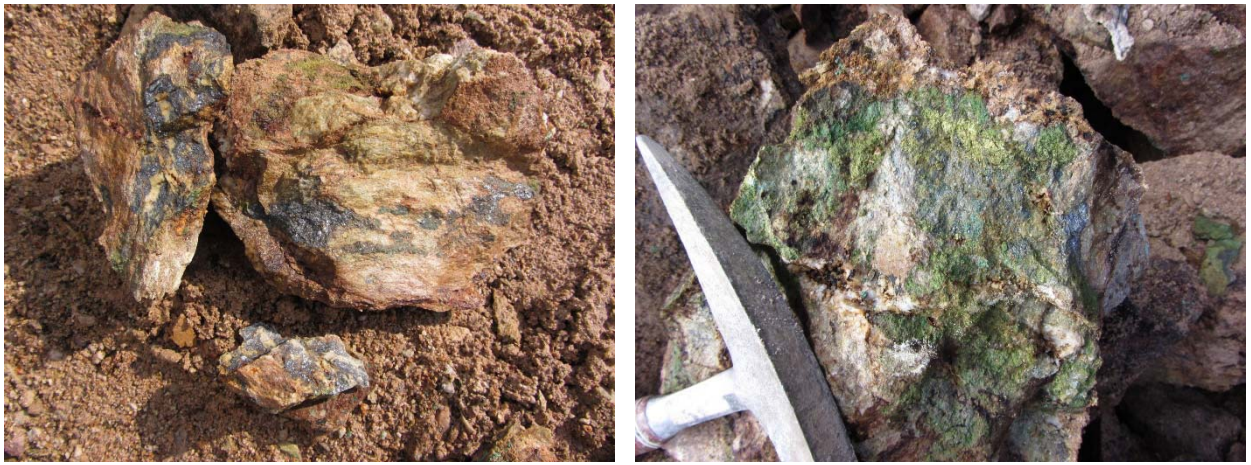

594

595

596 Figure 4:

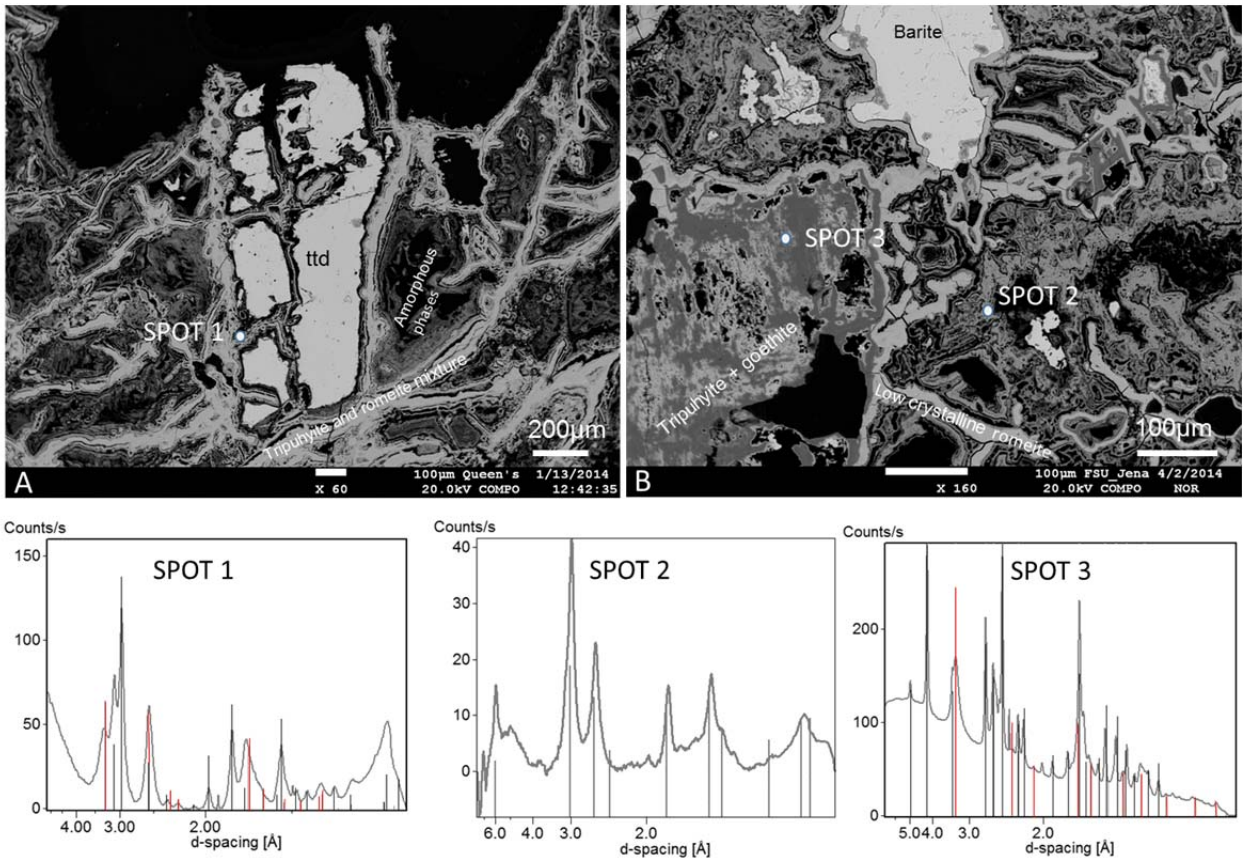

597

598

599 Figure 5:

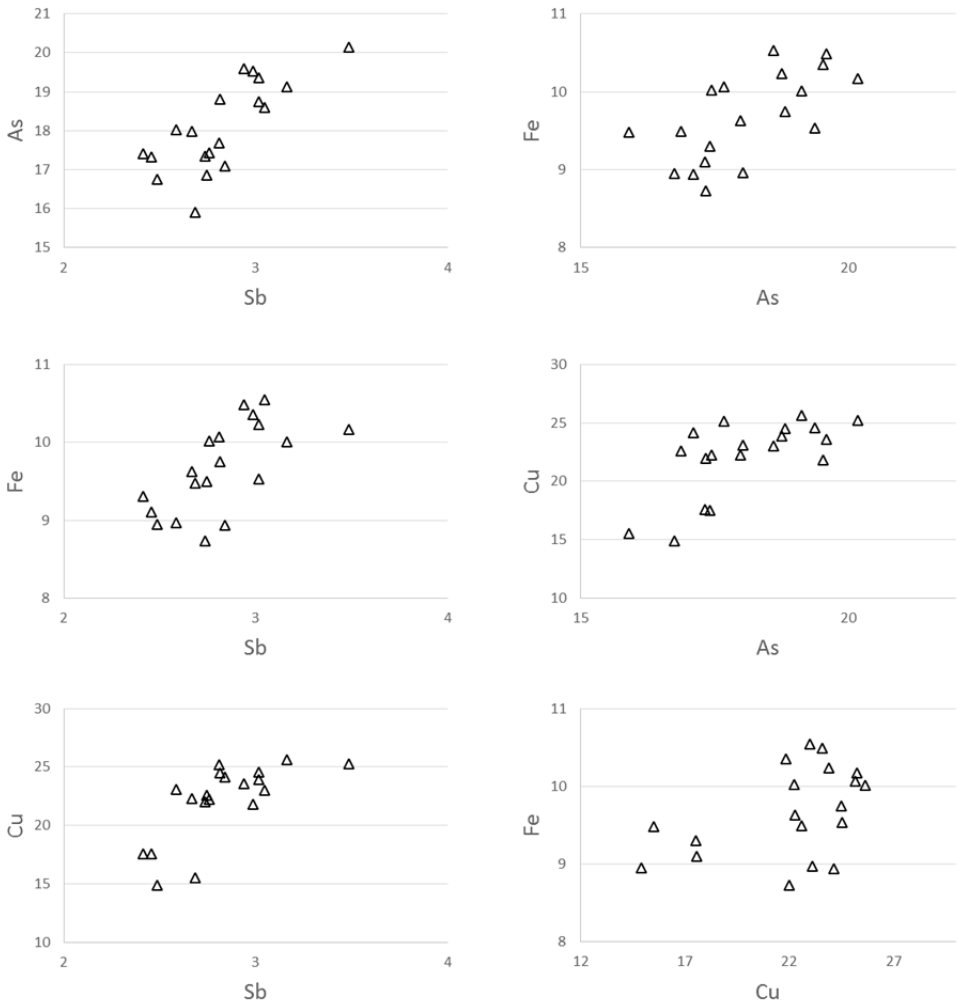

600

601

602 Figure 6:

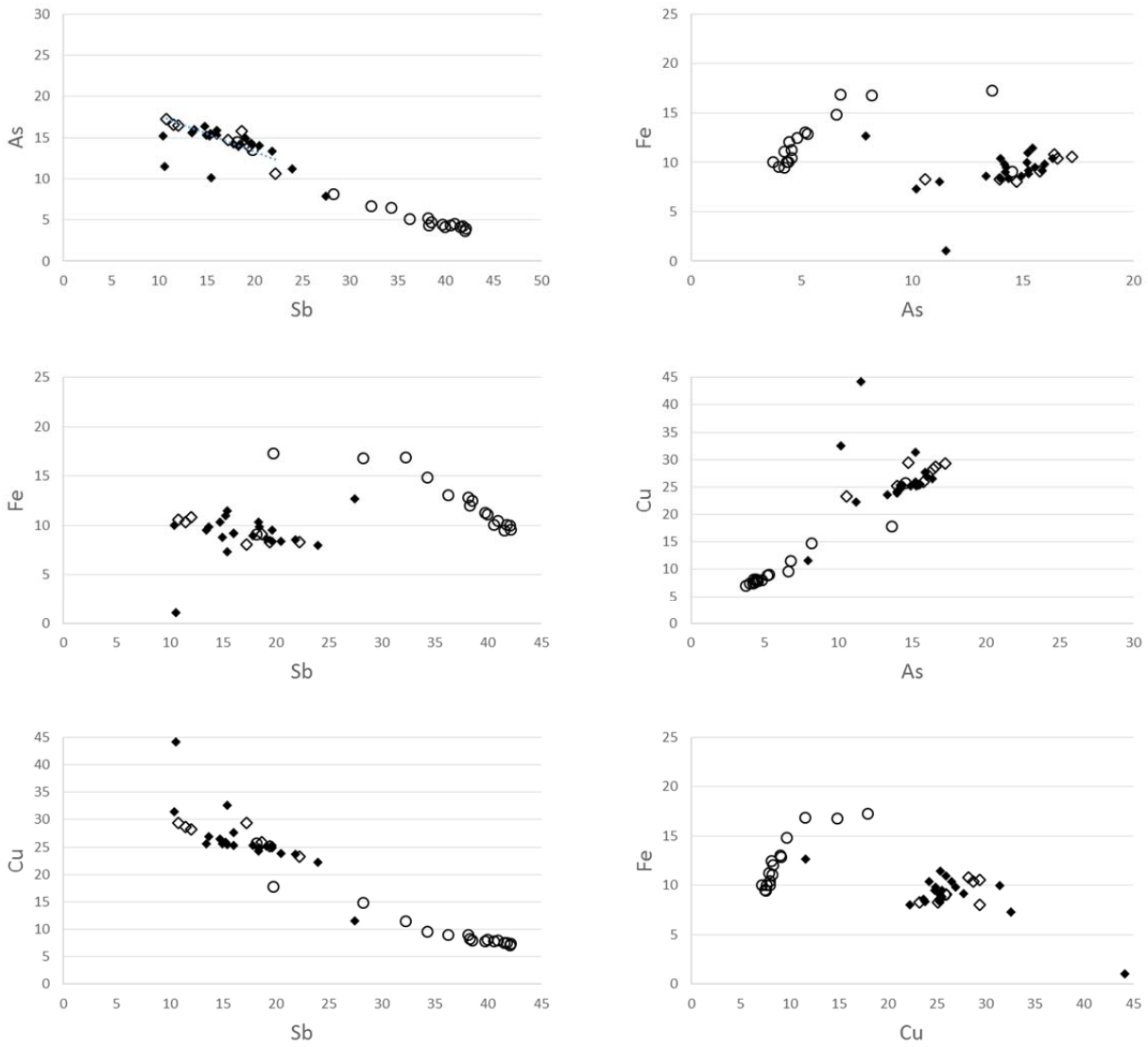

603

604 Figure 7:

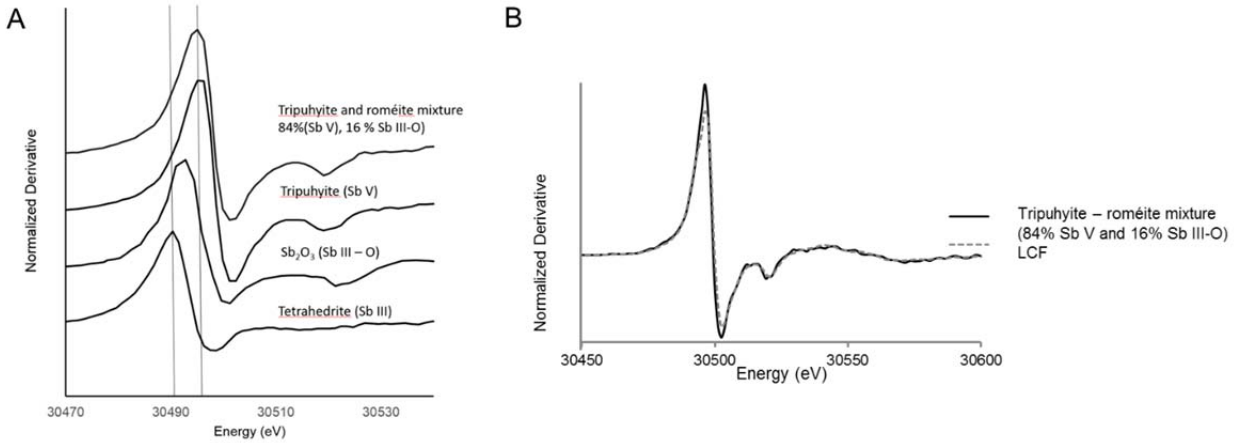

605

606

607

This is a preprint, the final version is subject to change, of the American Mineralogist (MSA)
Cite as Authors (Year) Title. American Mineralogist, in press.
(DOI will not work until issue is live.) DOI: http://dx.doi.org/10.2138/am-2017-5616

608 Figure 8:

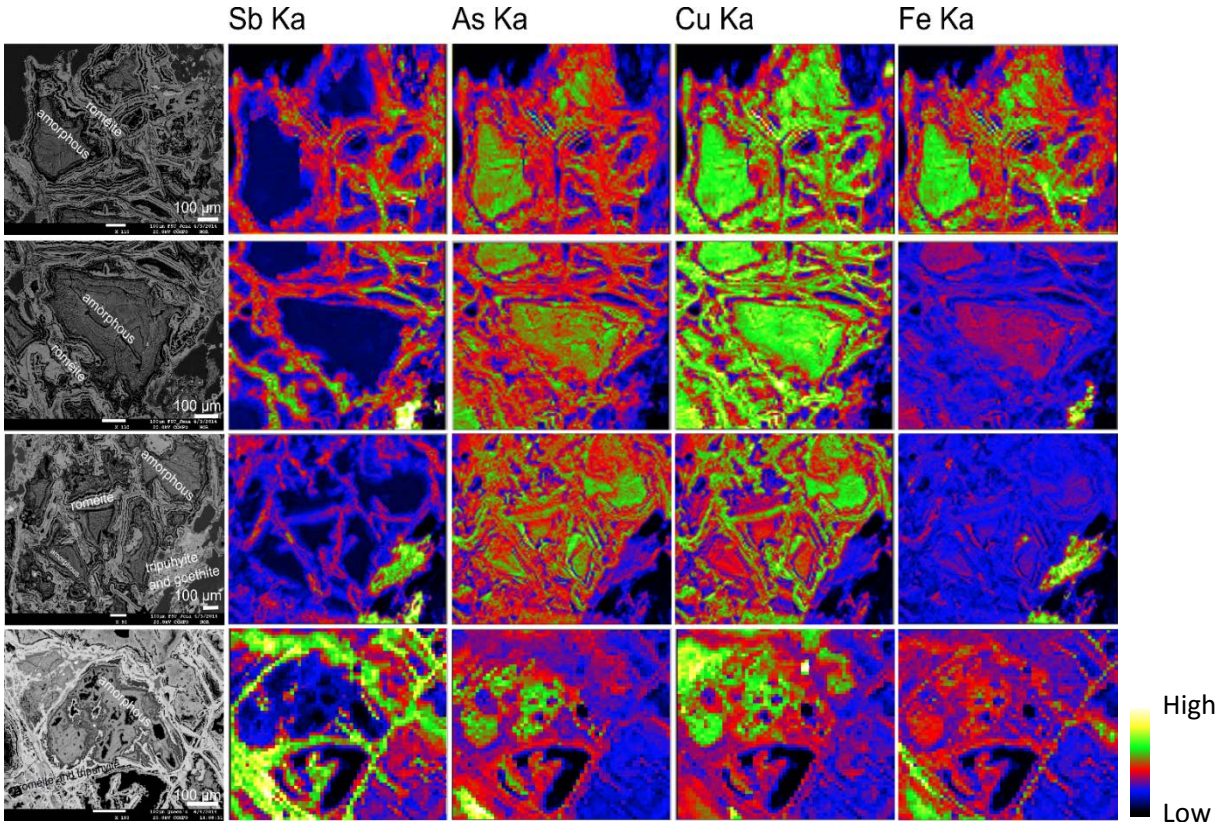

609

610

611

612

613

614 Figure 9:

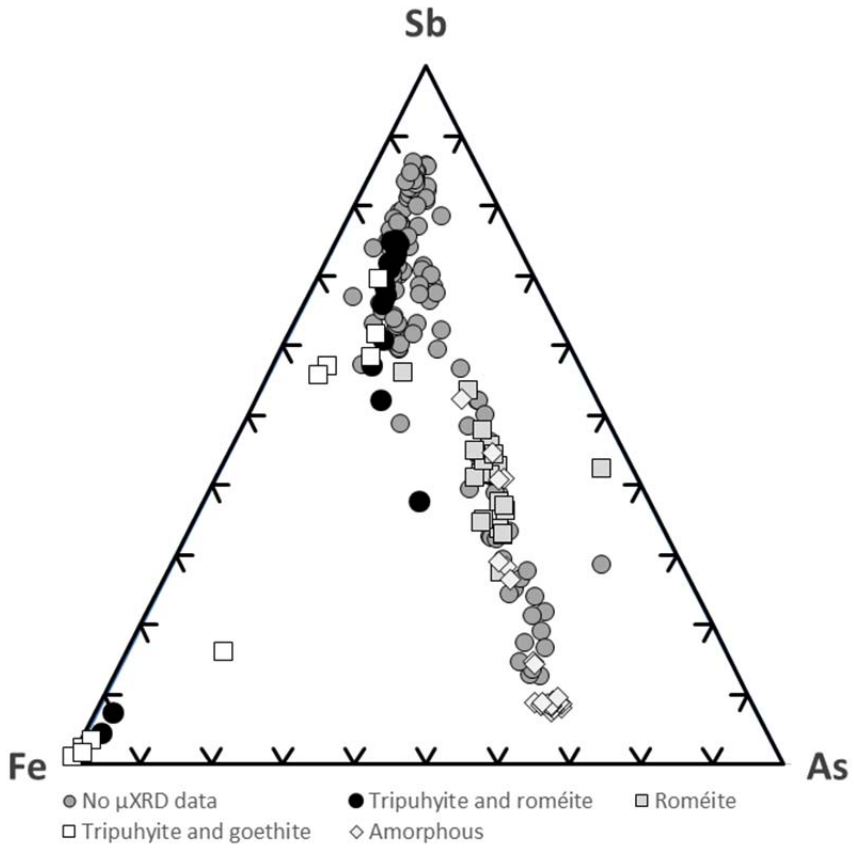

615

616

617 Figure 10:

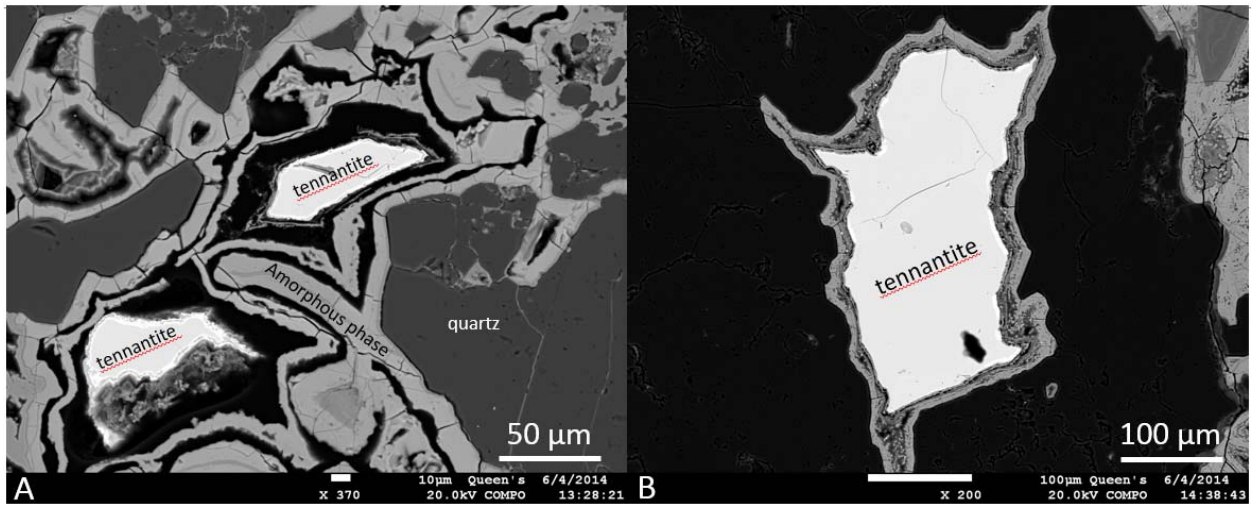

618